Brain, Behavior, & Immunity - Health 18 (2021) 100398

Contents lists available at ScienceDirect

Brain, Behavior, & Immunity - Health

journal homepage: www.editorialmanager.com/bbih/default.aspx

Astrocyte-derived microparticles initiate a neuroinflammatory cycle due to carbon monoxide poisoning

Deepa Ruhela, Veena M. Bhopale, Sudhakar Kalakonda, Stephen R. Thom *

Department of Emergency Medicine, University of Maryland School of Medicine, USA

ARTICLE INFO

Keywords:
Astrocyte
Thrombospondin-1
Neutrophil
Myeloperoxidase
CD36
Glymphatics
Acetyl-lysyltyrosylcysteine
Aquaporin-4

ABSTRACT

We hypothesized that carbon monoxide (CO) establishes an inflammatory cycle mediated by microparticles (MPs). Mice exposed to a CO protocol (1000 ppm for 40 min and then 3000 ppm for 20 min) that causes neuroinflammation exhibit NF-κB activation in astrocytes leading to generation of MPs expressing thrombospondin-1(TSP-1) that collect in deep cervical lymph nodes draining the brain glymphatic system. TSP-1 bearing MPs gain access to the blood stream where they activate neutrophils to generate a new family of MPs, and also stimulate endothelial cells as documented by leakage of intravenous 2000 kDa dextran. At the brain microvasculature, neutrophil and MPs sequestration, and myeloperoxidase activity result in elevations of the p65 subunit of NF-κB, serine 536 phosphorylated p65, CD36, and loss of astrocyte aquaporin-4 that persist for at least 7 days. Knock-out mice lacking the CD36 membrane receptor are resistant to all CO inflammatory changes. Events triggered by CO are recapitulated in naïve wild type mice injected with cervical node MPs from CO-exposed mice, but not control mice. All MPs-mediated events are inhibited with a NF-κB inhibitor, a myeloperoxidase inhibitor, or anti-TSP-1 antibodies. We conclude that astrocyte-derived MPs expressing TSP-1 establish a feed-forward neuroinflammatory cycle involving endothelial CD36-to-astrocyte NF-κB crosstalk. As there is currently no treatment for CO-induced neurological sequelae, these findings pose several possible sites for therapeutic interventions.

1. Introduction

Carbon monoxide (CO) is a common world-wide poison estimated to effect ~137 people per million annually, although incidence is higher in some developing countries (CDC, 2007; Mattiuzzi and Lippi, 2020; Raub et al., 2000). Hospital visits in the US number ~50,000/year, with ~1300 deaths (CDC, 2007; Hampson, 2016a,b). Cognitive, psychological, vestibular and motor impairments occur in ~25–50% of survivors from severe CO poisoning (Hampson et al., 2012; Rose et al., 2017). The etiology for neurological deficits that arise from days to weeks after poisoning remains unclear, as risk correlates poorly with hypoxic stress assessed by blood carboxyhemoglobin (COHb) levels (Raub et al., 2000). Patients with neurological sequelae show gradations of demyelination and cerebral white matter changes by magnetic resonance imaging (MRI) with elevations of myelin basic protein (MBP) in cerebrospinal fluid (Beppu et al., 2012; Ide and Kamijo, 2009; Kamijo et al., 2007; Kuroda et al., 2016). In the US, CO-induced neurological sequelae cost over $1 billion annually for direct hospital care and lost earnings (Hampson, 2016).

Our investigation used a murine model previously shown to involve MBP alterations leading to neurological dysfunction and explored the role of inflammatory microparticles (MPs) in CO poisoning (Han et al., 2007; Thom et al., 2004, 2006). MPs are one of a variety of so-called extracellular vesicles that play roles in cell-to-cell communication and inflammation (Mause and Weber, 2010). CO neuropathology can be transmitted to naïve mice by injections of MPs isolated from the blood of CO-poisoned mice (Xu et al., 2013). Neutrophils are involved with the MPs insults because myeloperoxidase (MPO) null knockout mice are resistant to injuries from MP infusions (Xu et al., 2013). MPs are 0.1–1 μm diameter vesicles generated by the outward budding of plasma

Abbreviations: acetyl-lysyltyrosylcysteine, KYC; Aquaporin-4, AQP4; Carboxyhemoglobin, COHb; Carbon monoxide, CO; Glial fibrillary acidic protein, GFAP; Magnetic resonance imaging, MRI; Microparticles, MPs; Myelin basic protein, MBP; Myeloperoxidase, MPO; Neuronal pentraxin receptor, NPR; Nod-like receptor pyrin containing 3, NLRP3; Nuclear factor- κB, NF-κB; Phosphate buffered saline, PBS; Phosphatidylserine, (PS); Thrombospondin-1, TSP-1; Transmembrane protein119, TMEM; 4-methyl-N1-(3-phenyl-propyl)-benzene-1,2-diamine, JSH-23.

* Corresponding author. Department of Emergency Medicine, University of Maryland School of Medicine, 655 W. Baltimore St., Bressler Research Building Room 4-013, Baltimore, MD, 21201, USA.

E-mail address: sthom@som.umaryland.edu (S.R. Thom).

https://doi.org/10.1016/j.bbih.2021.100398
Received 24 August 2021; Received in revised form 23 November 2021; Accepted 24 November 2021
Available online 27 November 2021

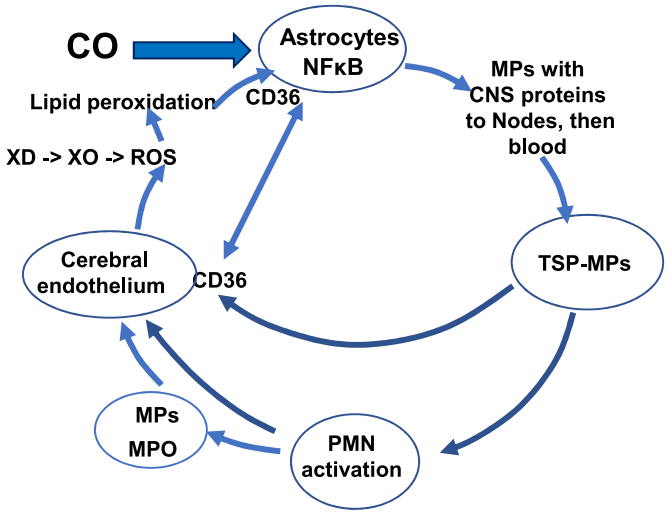

Fig. 1. Schematic showing sequence of events triggered by CO. CO triggers NF-κB activation in astrocytes (inhibited by JSH-23). GFAP/TSP-1 bearing MPs are produced and pass through the glymphatic system, enter the blood stream and activate endothelium along with neutrophils that, in turn, generate new MPs. CD36 is involved as the receptor for MPs on endothelium, also probably on astrocytes and microglia (shown as double arrow). MPO from the newly generated MPs and sequestered neutrophils cause perivascular oxidative stress reflected as production of reactive oxygen species (ROS) that is inhibited by KYC, along with a contribution from endothelial xanthine dehydrogenase (XD) conversion to oxidase (XO) and lipid peroxidation based on prior studies (Thom, 1992). These events lead to loss of AQP4 and maintenance of the inflammatory cycle due to continued CD36-mediated NF-κB activation.

membrane from virtually any cell, and they can be found in all body fluids. CNS-generated MPs can collect in the deep cervical lymph nodes and some are liberated to the blood stream (Ruhela et al., 2020).

Neutrophil activation occurs in acutely CO poisoned patients (Thom et al., 2006). This also occurs in our murine model and drives cerebral microvascular oxidative stress causing alterations in MBP that, in turn, lead to an adaptive immunological response and functional neurological deficits (Han et al., 2007; Thom et al., 2004, 2006). Events are abrogated by neutropenia, antioxidants or inhibiting neutrophil adherence. There is no explanation for why neutrophils are activated, why they appear to target the neurovasculature, nor how neuroinflammation is perpetuated so that functional deficits are manifested weeks after CO exposure.

CO is well known to cause oxidative stress that is in part due to mitochondrial dysfunction (Raub et al., 2000). In brain, astrocytes respond to oxidative stress with NF-κB activation which, among other events, results in generation of thrombospondin (TSP)-1 and −2 and a variety of extracellular vesicles (Verkhratsky et al., 2016). TSP-1 is a neurogenic factor and can protect mitochondrial functions, while TSP-2 plays a role in blood-brain barrier repair (Kang et al., 2018; Lu and Kipnis, 2010; Tian et al., 2011). However, TSP-1 engagement by several varieties of leukocytes will cause priming, chemotaxis, NLRP3 inflammasome formation/interleukin -1β production, enhanced endothelial attachment and spreading (Majluf-Cruz et al., 2000; Martin-Manso et al., 2000).

We hypothesized that early intra-CNS responses to CO would be reflected by changes in the MPs that exit the brain via the glymphatic system. Once these MPs gain access to the blood stream, they could activate neutrophils due to expression of proteins such as TSP-1. TSP-1 receptors on neutrophils include Toll-like receptor-4, CD47, and integrins (Greenwalt et al., 1992; Majluf-Cruz et al., 2000). Neutrophil activation can cause NLRP3 assembly, which is linked to MPs production (Thom et al., 2014, 2017a, 2017b). Therefore, TSP-1 engagement would generate additional MPs and perivascular CNS inflammation could be exacerbated by activated, adherent neutrophils and the new neutrophil-derived MPs, as has been shown for other insults (Thom et al., 2011). Thus, we hypothesized that astrocyte-generated MPs could drive neuropathology beyond that due to the direct impact of CO on brain oxidative metabolism.

Astrocytes are intimately involved with the glymphatic system (Absinta et al., 2017; Iliff et al., 2012). Cerebrospinal fluid (CSF) enters the brain parenchyma via aquaporin (AQP)-4 water channels located in astrocyte end-feet that encircle the brain vasculature. CSF mixes with parenchymal interstitial fluid, drains via perivenous spaces and ultimately via connections with cervical lymphatic vessels exits through the deep cervical lymph nodes (Holter et al., 2017). Progressive neuroinflammation from a variety of insults leads to loss of AQP4, damaged lymphatic channels with glymphatic dysfunction, and neurocognitive deficits that correlate with diminished glymphatic flow (Weller et al., 2008).

Included in our thinking was a possible role for CD36, a class B pattern recognition receptor expressed in many tissues and found of microvascular endothelium, macrophages, B lymphocytes, and platelets (Greenwalt et al., 1992; Silverstein and Febbraio, 2009; Won et al., 2008). In healthy brain, CD36 is found predominantly on endothelial cells and after ischemic insults expression occurs on astrocytes and microglia over a span of 6 h to 3 days (Cho et al., 2005; Febbraio and Silverstein, 2007). CD36 expression is increased in brain by oxidative stress and endothelial engagement enhances NF-κB activation, inflammatory pathways and neutrophil recruitment (Bai et al., 2020; Ghosh et al., 2008; Kim et al., 2015; Kunz et al., 2008). CD36 will bind phosphatidylserine (PS) and facilitate MPs adherence to endothelium because PS is highly expressed on the MPs surface (Bai et al., 2020; Ghosh et al., 2008). CD36 ligands include TSP-1, polyanionic lipids, lipoproteins, and advance glycation end products (Febbraio and Silverstein, 2007).

Here we demonstrate that CO poisoning establishes a cyclic, feed-forward process allowing neuroinflammation to continue for weeks after an acute exposure. The process develops as follows: CO → astrocyte NF-κB →MPs expressing TSP-1 to cervical nodes, then blood → neutrophil activation with new MPs → brain endothelium sequesters TSP-1 expressing MPs and neutrophils that exacerbate oxidative stress → additional CD36 expression maintains astrocyte NF-κB activation and neuroinflammation. This process is illustrated in Fig. 1 and interventions we utilized are summarized in the caption. By comparing effects between CO-exposed mice and naïve mice injected with MPs isolated from the cervical lymph nodes of CO-exposed mice we demonstrate that these particles as the proximal mediator of brain-to-blood-to-brain communications. Given that CO-induced neurological sequelae develop days-to-weeks after acute poisoning, these findings offer possible interventions to this currently incurable affliction.

2. Materials and methods

2.1. Materials

Chemicals were purchased from Sigma-Aldrich (St. Louis, MO) unless otherwise noted. CO at 1000 or 3000 ppm in air was purchased from Air Products and Chemicals, Inc. (Allentown, PA). Antibodies were validated from the purchase company with indicated host specificity and the data sheets of each product were supplied as below: Anti-annexin V-PE (Becton Dickinson/Pharmingen, BD, San Jose, CA cat # 556421), anti-actin (Sigma-Aldrich, St. Louis, Mo, cat# A-2066), anti-AQP4 (Millipore/Sigma, St. Louis, MO, cat#ab3594), anti-CD36 (Genetex, Irvine, CA, cat# GTX20003), anti-Ly6G eFluor450 (Novus Biologicals, Centennial, CO, cat#RB6-8C5), anti-mouse MPO-PE (R & D Systems, Minneapolis, MN, cat# AF3667), anti-mouse CD31 BV510 (BD cat#563089), anti-CD41 PerCP Cy5.5 (BioLegend, San Diego, CA, cat#133918), Anti-GFAP Brilliant Violet 421 (BioLegend, cat# 644719), anti-TMEM119-APC (Abcam, Cambridge, UK, cat#ab225494), anti-NPR AF-790 (Santa Cruz Biotechnology, Dallas, TX cat# sc-390081), anti-MBP PerCP (Novus Biologicals, cat # NBP2–22121PCP), anti-TSP-1 (Santa Cruz,

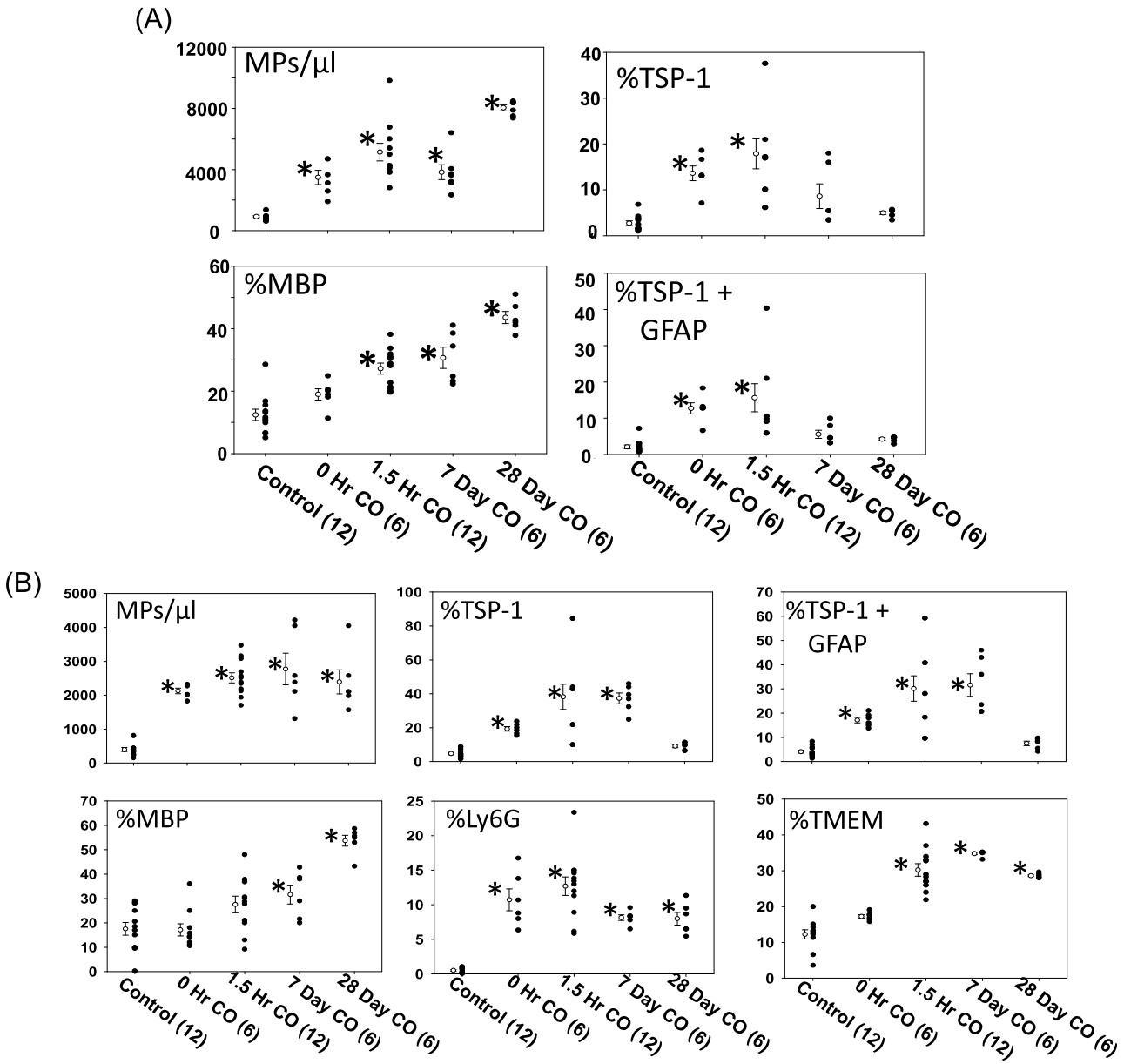

Fig. 2. Flow cytometry analyzed MPs showing statistically significant differences from control are shown for cervical lymph nodes (A) and blood samples (B). Data show the total number of MPs/µl plasma (blood) or uniformly prepared cell suspension (nodes) – see section 2.3 for methods, and the percent of MPs expressing proteins summarized in section 3.1. The open circles show mean ± SE (sample numbers are listed at the bottom of the figure) with * indicating those statistically significantly different from control ($p < 0.05$, ANOVA). Solid circles show individual data points for control and samples obtained from mice exposed to CO and then euthanized immediately, 1.5 h, 7 or 28 days after exposure.

Table 1
MPs subtypes found to not be altered by CO exposure. Data show the percent of MPs expressing proteins described in section 3.1.

Node MPs	% GFAP	%TMEM	%NPR
Control (12)	49.8 ± 2.8	14.0 ± 2.6	21.5 ± 1.9
CO-0 H(6)	55.9 ± 7.2	17.2 ± 5.3	14.7 ± 1.6
CO-1.5H(12)	49.4 ± 3.8	21.8 ± 6.6	25.8 ± 2.9
CO-7D (6)	51.8 ± 3.7	25.4 ± 2.4	22.4 ± 1.8
CO28D (6)	63.3 ± 1.1	28.9 ± 0.4	34.8 ± 1.4

Blood MPs	% GFAP	%NPR	%CD41	% ECs
Control (12)	41.2 ± 2.0	20.9 ± 2.2	8.2 ± 1.8	0.9 ± 0.3
CO-0 H(6)	48.7 ± 4.1	17.3 ± 2.6	5.2 ± 0.8	1.0 ± 0.2
CO-1.5H(12)	47.8 ± 3.0	25.2 ± 3.3	11.3 ± 2.9	1.8 ± 0.9
CO-7D (6)	48.2 ± 4.4	26.7 ± 4.0	6.3 ± 1.1	0.7 ± 0.2
CO28D (6)	39.6 ± 2.6	34.6 ± 5.3	9.5 ± 2.3	0.9 ± 0.3

cat#393504 and 393504FITC), anti-p65 subunit of NF-κB (Abcam, cat# ab32536), anti-phosphorylated at serine 536 (Phospho-Ser^{536}) p65 NF-κB) (Cell Signaling, Danvers, MA, cat# 3031).

2.2. Animals

All aspects of this study were reviewed and approved by the Institutional Animal Care and Use Committee. All experiments were performed using young, adult (10–12 weeks) mice with approximately equal numbers of males and females in all experimental groups. C57BL/6J mice *(Mus musculus)* were purchased from Jackson Laboratories (Bar Harbor, ME) and housed in the university animal facility. CD36 knock-out (KO) mice were initially purchased from Jackson Labs and a colony was raised in the University vivarium.

Mice were housed in the university animal facility with a 12/12 h

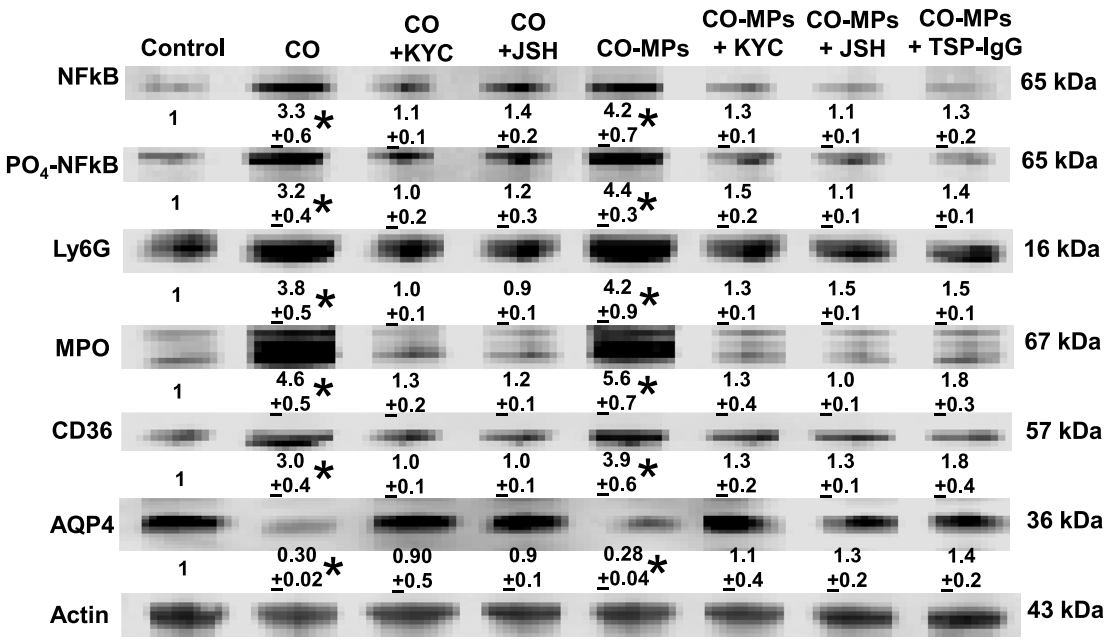

Fig. 3. Western blots of brain homogenates from control mice and those euthanized 1.5 h after CO exposure. Lanes indicate control (lane 1), post-CO (lane 2), a mouse injected with the myeloperoxidase inhibitor, KYC then exposed to CO and euthanized 2 h later (lane 3), a mouse injected with the NF-κB inhibitor, JSH-23, then exposed to CO and euthanized 1.5 h later (lane 4), a naïve mice injected with MPs isolated from cervical lymph nodes of a CO-exposed mouse (CO-MPs, lane 5), a naïve mouse injected with KYC and then CO-MPs (lane 6), a naïve mouse injected with JSH-23 and then CO-MPs (lane 7), and a naïve mouse injected with CO-MPs that had been incubated with IgG to TSP-1 (lane 8). This is a representative blot with mean ± SE values shown beneath each band expressed as fold-change from control for replicate studies. Normalization of band densities to β actin in the same samples were performed for daily experiments and then values for experimental groups were expressed as a ratio against the control value (thus control is shown as 1.0). Replicate sample numbers were: Control, n = 10: CO, n = 10; CO + KYC, n = 4; CO + JSH, n = 4; CO-MPs, n = 5; CO-MPs + KYC, n = 4; CO-MPs + JSH, n = 4; CO-MPs + TSP IgG, n = 5. The * symbol indicates $p < 0.05$ versus the control, ANOVA.

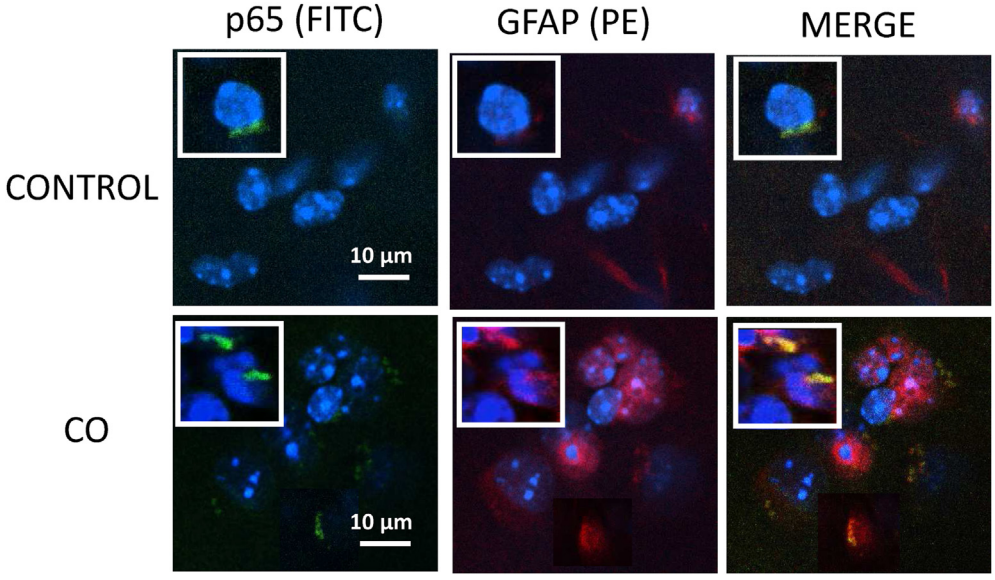

Fig. 4. Representative images from cerebral cortex of a control mouse and one euthanized 1.5 h after CO exposure. Sections were stained with antibodies to GFAP (red), NF-κB p65 protein (green) and nuclei using DAPI (blue). The main images are at 60x magnification with the insert as 120x to better show p65 colocalization with nuclei. (For interpretation of the references to color in this figure legend, the reader is referred to the Web version of this article.)

light-dark cycle. Housing and all experiments were conducted at 22–24 °C and 40–70% humidity. Mice received water *ad libitum* and were fed Laboratory Rodent Diet 5001 (PMI Nutritional Inc., Brentwood, MO). Mice were left to breathe room air (control) or subjected to 1-h exposure to CO according to an established model of 1000 ppm for 40 min and 3000 ppm for 20 min. In prior studies we demonstrated that this exposure achieves a blood carboxyhemoglobin level of 54% (Thom, 1990; Thom et al., 2004). COHb assays were not replicated in the current investigation.

Randomization of mice for experimentation was performed by first collecting all mice to be used on a day into a single plastic cage and then randomly selecting an individual mouse for use as the daily control or for an intervention group. Studies were done over a span of 9 months with acclimatized mice purchased in groups of 6–12 at bi-weekly intervals or

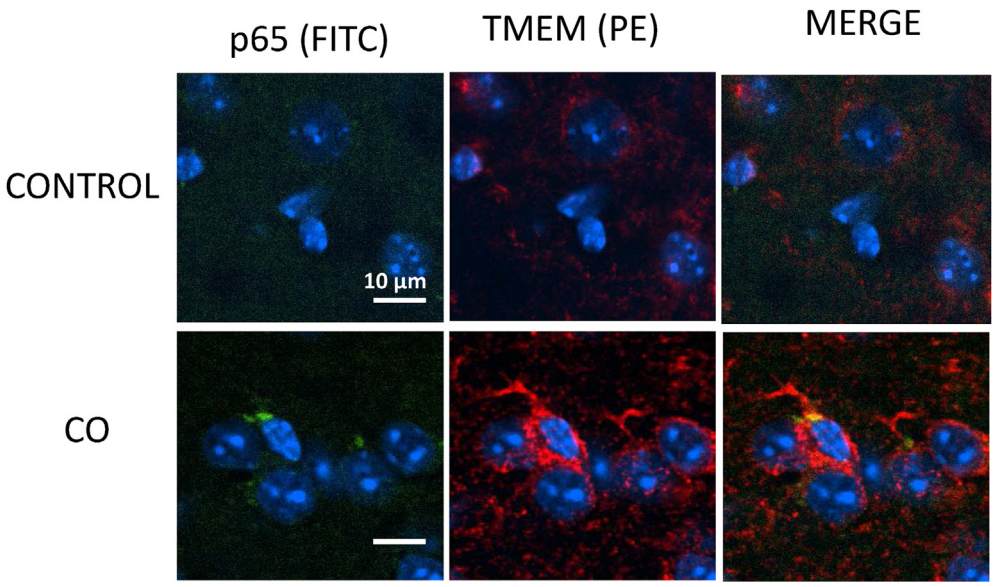

Fig. 5. Representative images from cerebral cortex of a control mouse and one euthanized 1.5 h after CO exposure. Sections were stained with antibodies to TMEM-119 (red), NF-κB p65 protein (green) and nuclei using DAPI (blue). Images are at 60x magnification. (For interpretation of the references to color in this figure legend, the reader is referred to the Web version of this article.)

in the case of CD36 KOs, when mature. Mice were used according to a block design where individual blocks represented mice selected as control or CO-exposure, and then with further experimentation including infusion of an agent.

Groups of 6–12 mice were anesthetized and euthanized for blood and tissue collection at times points chosen based on the time course for events in prior work. Thus, mice were exposed to CO and euthanized immediately, 90 min, 7 days or 28 days later. Neutrophil sequestration along the neurovasculature can be documented immediately following the 1-h exposure followed by oxidant generation, lipid peroxidation and structural alterations to MBP that occur by 90 min post-exposure, CD4 lymphocyte influx by 1 week and functional neurological deficits are apparent 28 days after poisoning (Han et al., 2007; Ischiropoulos et al., 1996; Thom, 1992, 1993; Thom et al., 1995, 1999, 2004, 2006; Xu et al., 2013). Because pathological events occur promptly in response to CO, interventions were administered at 30 min prior to CO exposure. These included intraperitoneal (IP) injections of 3 mg/kg 4-methyl-N1-(3-phenyl-propyl)-benzene-1,2-diamine (JSH-23), an inhibitor of NF-κB nuclear translocation, or 0.3 mg/kg acetyl-lysyltyrosylcysteine (KYC), a tripeptide inhibitor of MPO (Kumar et al., 2011; Shin et al., 2004; Zhang et al., 2016). Interventions were studied in groups of 4–8 mice.

Data were scored and analyzed in a blinded manner such that the scorer did not know an animal's group assignment. All mice involved in this project were included in data analysis, none were excluded. To minimize animal usage and maximize information gain, experiments were largely designed to utilize both blood and tissue from the same animals. Mice were anesthetized [intraperitoneal administration of ketamine (100 mg/kg) and xylazine (10 mg/kg)] skin was prepared by swabbing with Betadine and blood was obtained into heparinized syringes by aortic puncture, prior to tissue harvesting.

2.3. Cervical lymph node MPs acquisition and analysis

Cervical lymph nodes were identified and removed from mice as described previously (Ruhela et al., 2020). Nodes (2–6) from a mouse were weighed, placed in a Petri dish and finely cut to pieces with a scalpel. The minced nodes were suspended as 20 µg/ml digestion buffer (DMEM, 2% FBS containing 250 µg dispase) and incubated for 30 min at 37 °C with vortexing at 15-min intervals. Tissue aggregates were then broken up by repeated passage through a narrow, flamed tip Pasteur pipette and 0.1 ml of 50 mM EDTA per ml of node suspension was added to aid dispersion of the particles. After 10-min incubation the suspension was diluted 1.6-fold with PBS and passed through a 40 µm filter. The suspension was then centrifuged at 600×*g* for 5 min, the pellet discarded, and re-centrifuged at 15,000g for 30 min. MPs in the supernatant were then analyzed. Detailed methods along with representative box plots showing flow cytometry enumeration strategy are published (Ruhela et al., 2020).

2.4. Blood MP acquisition and processing

Blood-borne MPs were isolated and prepared for analysis by flow cytometry as previously described (Ruhela et al., 2020; Thom et al., 2011). Briefly, heparinized blood was centrifuged for 5 min at 1500 g. EDTA was added to the supernatant to achieve 12.5 mM to prevent MPs aggregation, centrifuged at 15,000 g for 30 min, and supernatant used for analysis. Examples of blood-borne MPs flow cytometry enumeration strategy have been published previously (Bhullar et al., 2016).

2.5. MPs for re-injection

MPs donor mice were exposed to the 1-h CO protocol and euthanized 1.5 h later. Cervical node MPs were isolated as described in section 2.3. The 15,000 g supernatant was parceled among centrifuge tubes at a ratio of 250 µl + 4 ml phosphate buffered saline (PBS) and centrifuged at 100,000 g for 60 min (typically 3–4 tubes/experiment were used). Supernatant (4 ml) was then carefully removed and the pellet containing the MPs resuspended in sterile PBS. The MPs were counted and diluted so that 60,000 MPs in 200 µl PBS was intravenous injected via a tail vein into naïve mice. Recipient mice were then euthanized 1.5 h later to evaluate changed in MPs in cervical lymph nodes and blood, vascular permeability and neutrophil activation as described below. Where indicated, some mice were injected IP with the NF-κB inhibitor, JSH-23, or the MPO inhibitor, KYC as described in section 2.2, 30 minutes prior to MPs injections and in other groups, MPs were first combined for 30 min with 5 µg anti-TSP antibodies.

2.6. MP analysis

All reagents and solutions used for MP isolation and analysis were

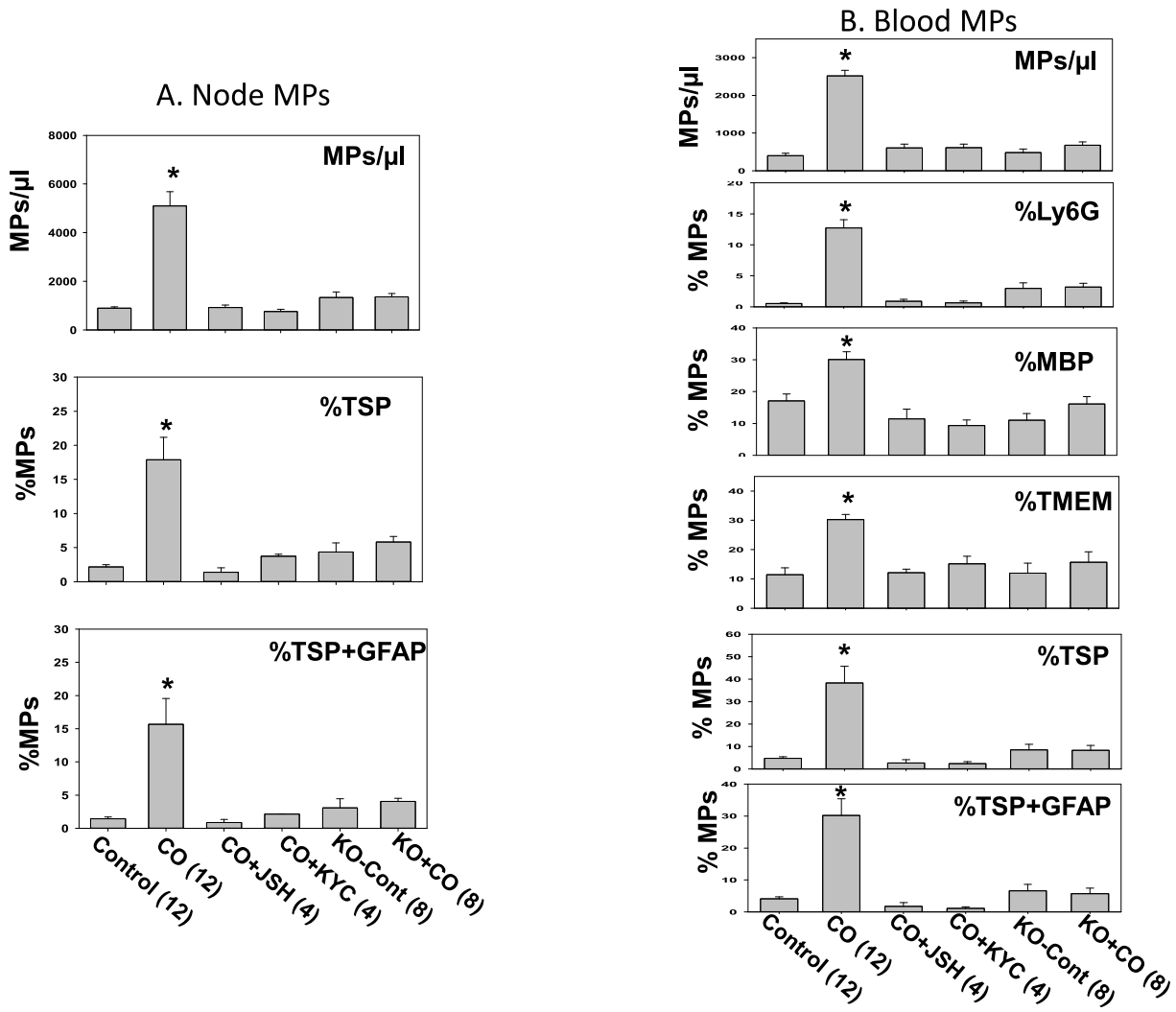

Fig. 6. Flow cytometry analyzed MPs counts for cervical lymph nodes (A) and blood samples (B) from wild type control mice, and those exposed to CO without and with JSH-23 or KYC and euthanized 1.5 h later. The last two columns in each figure show data from CD36 knock-out (KO) mice exposed only to air (Cont = control) or to CO. Data are mean ± SE with the number of replicates shown. The * symbol indicates $p < 0.05$ versus the control, ANOVA. Box plots rather than dots as in Fig. 2 were used to ease the ability to assess the differences among groups.

filtered with 0.1 µm filter (EMD Millipore, Billerica, MA). MPs were analyzed as described previously (Thom et al., 2011; Yang et al., 2012). In brief, flow cytometry was performed with an 8-color, triple laser MACSQuant® Analyzer (Miltenyi Biotec Corp., Auburn, CA) using MACSQuantify™ software version 2.5 to analyze data. MACSQuant was calibrated every other day with calibration beads ((Miltenyi Biotec Corp., Auburn, CA). Forward and side scatter were set at logarithmic gain. Photomultiplier tube voltage and triggers were optimized to detect sub-micron particles. Micro-beads of 3 different diameters 0.3 µm (Sigma, Inc., St. Louis, MO), 1.0 µm and 3.0 µm (Spherotech, Inc., Lake Forest, IL) were used for initial settings and before each experiment as an internal control. Samples were suspended in Annexin binding buffer solution (1:10 v/v in distilled water, (BD Pharmingen, San Jose, CA), and antibodies as listed above. All reagents and solutions used for MP analysis were sterile and filtered (0.1 µm filter). MPs were defined as annexin V-positive particles with diameters of 0.3–1 µm diameter. The concentration of MPs in sample tubes was determined by MACSQuant® Analyzer according to exact volume of solution from which MPs were analyzed.

2.7. Neutrophil activation analysis

Whole fixed blood (100 µl) was stained for 30 min at room temperature in the dark with optimized concentrations of Ly6G, MPO and CD18 antibodies as listed in section 2.1 following published methods (Thom et al., 2017b; Yang et al., 2013). After staining 2 ml phosphate buffered saline (PBS) was added to dilute each sample tube prior to analysis, with the cytometer acquisition set to use anti-mouse Ly6G as the fluorescence trigger to recognize mouse neutrophils.

2.8. Colloidal silica endothelium enriched tissue homogenates and vascular permeability assay

Mice were anesthetized, exsanguinated, perfused with phosphate buffered saline (PBS) to remove residual blood and then with lysine-fixable tetramethylrhodamine-conjugated dextran (2×10^6 Da, Invitrogen, Carlsbad, CA) followed by colloidal silica according to published methods (Thom et al., 2011; Yang et al., 2012). After centrifugation the endothelium enriched pellets were obtained for analysis from the brain

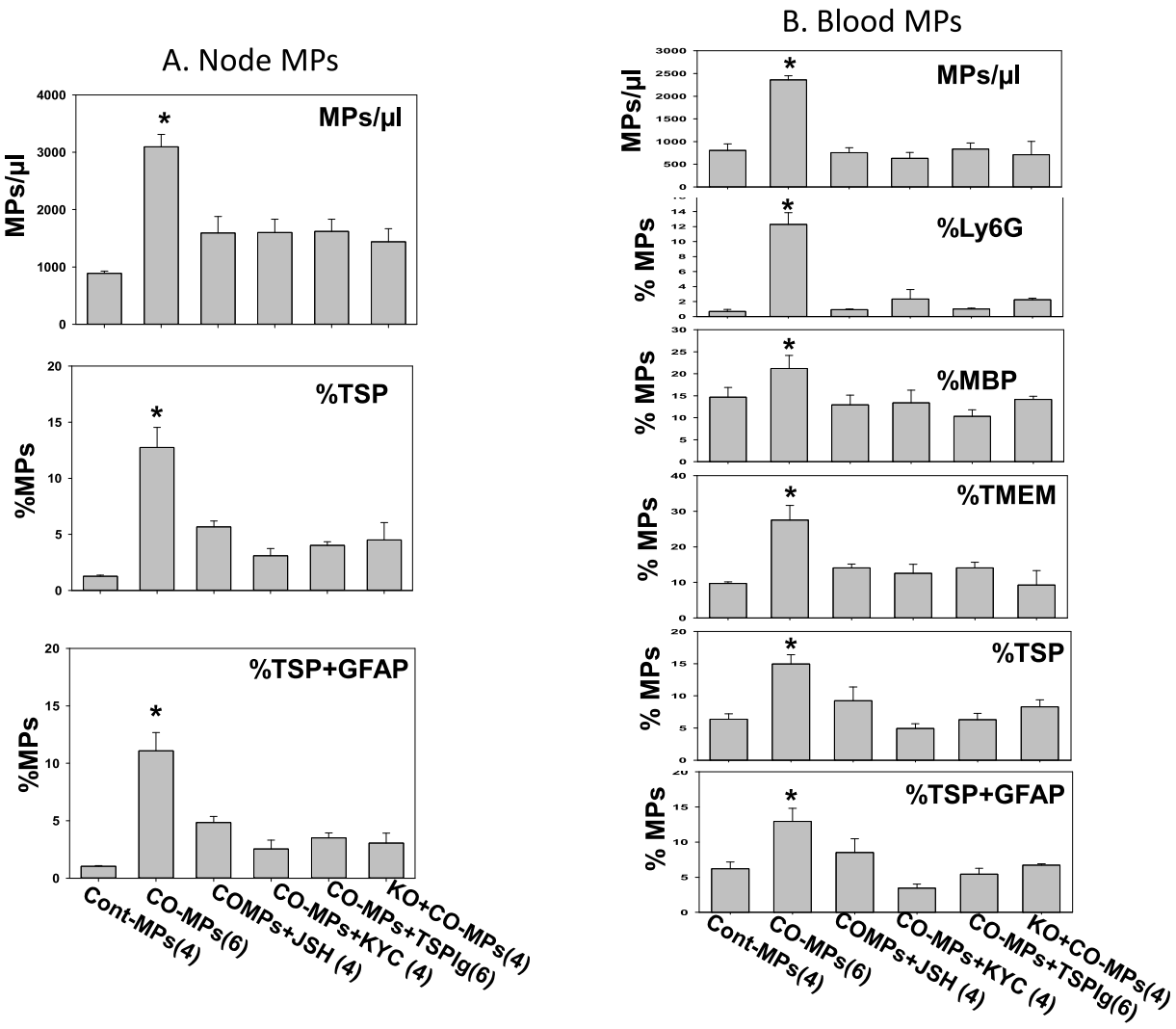

Fig. 7. Flow cytometry analyzed MPs counts for cervical lymph nodes (A) and blood samples (B) from mice injected with 60,000 cervical lymph node MPs and euthanized 1.5 h later. Columns show results for wild type naïve mice injected with node MPs from wild type control mice (Cont-MPs), those injected with node MPs isolated from wild type control mice 1.5 h after exposure to CO (CO-MPs), those injected with CO-MPs as well as JSH-23, those injected with CO-MPs as well as KYC, and those injected with CO-MPs that were first incubated with IgG to TSP-1. The last column in each figure show data from CD36 knock-out (KO) mice injected with CO-MPs. Data are mean ± SE with the number of replicates shown. The * symbol indicates $p < 0.05$ versus the control, ANOVA.

and leg skeletal muscle. Vascular leakage was quantified as rhodamine fluorescence after values were normalized to that obtained with a control mouse included in each experiment (Thom et al., 2011). Neutrophil sequestration was evaluated by performing Western blots on tissue homogenates, probing for Ly6G and MPO and normalizing band density to β-actin bands on the same blots following our published procedures (Thom et al., 2011; Yang et al., 2012).

2.9. Statistical analysis

Results are expressed as the mean ± standard error (SE) for four or more independent experiments with analysis using SigmaStat (Jandel Scientific, San Jose, CA). Data normality was assessed using the Shapiro-Wilk test. Statistical analysis in each assay is detailed in figure legends. For two group comparisons, a two-tailed, unpaired Student's *t*-test was used. For multiple group comparisons, a one-way analysis of variance (ANOVA) and Newman-Keuls post-hoc test was used. For all studies, the level of statistical significance was defined as $p < 0.05$.

3. Results

3.1. CO exposure causes elevations of MPs in cervical node and blood

Mice were exposed to CO as described in section 2.2 and euthanized immediately, 90 min, 7 days or 28 days later. MPs were identified based on size and surface expression of annexin V. Proteins probed on the surface of the MPs included those from neutrophils (Ly6G), platelets (CD41) and endothelial cells ($CD31^+$ and CD41-dim), astrocytes (glial fibrillary acidic protein, GFAP), microglia (transmembrane protein119, TMEM), oligodendroglia (myelin basic protein, MBP) and neurons (neuronal pentraxin receptor, NPR). As discussed in section 1, we also were interested in MPs that expressed TSP-1.

Fig. 2 A and B demonstrate the types of MPs in CO-exposed mice that were found to be statistically significantly different from control in the deep cervical lymph nodes and blood. TSP-1 expressing MPs in all mice node and blood samples from control and CO-exposed groups also expressed GFAP on 85.6 ± 1.9% (n = 74) of particles. MPs values in

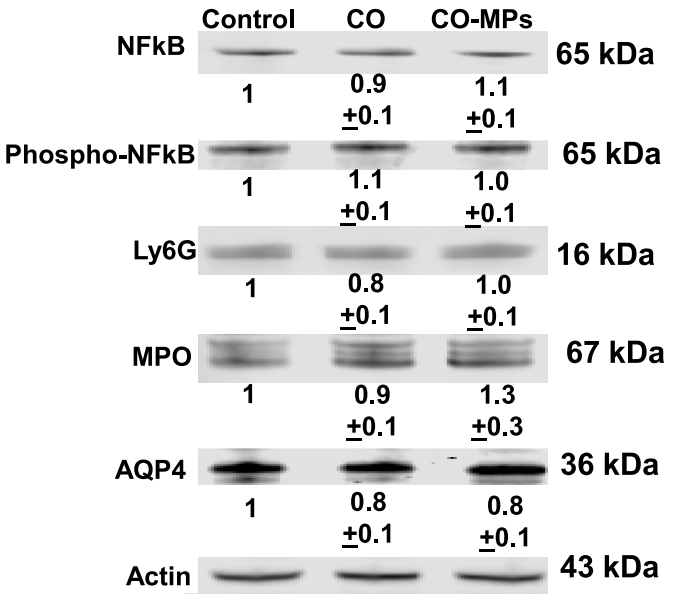

Fig. 8. CD36 knock-out mouse brain homogenate Western blots were performed for air-breathing control mice, those euthanized 1.5 h after CO exposure, and 1.5 h after intravenous injections of 60,000 cervical lymph node MPs from a wild type mouse exposed to CO (CO-MPs). This is a representative single blot with mean ± SE values shown beneath each band expressed as fold-change from control for replicate studies (n = 6 for each group), as described in the caption for Fig. 3. There were no significant differences between control and post-CO samples.

cervical nodes of all four CO-exposed (0 h, 1.5 h, 7 days and 28 days post-CO) groups demonstrated statistically significant increases in total number of particles and for the immediate and 1.5-h post-CO groups there were increases in MPs expressing TSP1 and co-expressing GFAP and TSP1. At 1.5 h, 7- and 28-days post-CO there were also significant differences from control for MPs expressing MBP. Blood from all CO-exposed groups exhibited elevations in total MPs number and MPs expressing Ly6G. At 1.5 h and 7 days post-CO there were also significant differences from control for MPs expressing TSP1, TSP1 plus GFAP, TMEM and MBP. At 28 days there were significant differences from control for MPs expressing TMEM and MBP. The subtypes of MPs that were not found different between control and CO-exposed groups are shown in Table 1.

3.2. Brain western blots show multiple protein changes post-CO

We were interested in evaluating the biochemical events related to early CO responses. Therefore, Western blots were prepared using brains perfused to remove intracranial blood as described in section 2.8. We used simple homogenates but found greater differences with homogenates from brains perfused with positively charged colloidal silica in a manner, as reported by others, to enrich samples for endothelium and adjacent cells including astrocytes (Beaulieu et al., 1997). Fig. 3 is a representative blot where, compared to control (lane 1), there were elevations of the p65 subunit of NF-κB, serine 536 phosphorylated (Phospho-Ser^{536}) p65 NF-κB, Ly6G, myeloperoxidase (MPO) and CD36 with loss of AQP4 at 1.5 h post-CO (lane 2). The numbers below the Western blot bands indicate mean ± SE band densities relative to the densities of control samples from replicate studies. Studies were also done with mice euthanized at 7 days post-CO. The relative band densities for most proteins at 7 days were virtually the same as at 1.5 h post-CO, except MPO which was greater than both control and the 1.5-h post-CO value ($p < 0.05$, ANOVA). Values expressed as fold-change from control at 7 days post-CO were as follows for 5 replicate studies: For p65 NF-κB, 2.6 ± 0.2, for Phospho-Ser^{536}p65 NF-κB, 2.0 ± 0.1, for Ly6G, 2.3 ± 0.2, for MPO 6.5 ± 0.3, for CD36 2.8 ± 0.06 and for AQP4 0.21 ± 0.06.

3.3. Immunocytochemical evidence of NF-κB elevations in brain

We used immunocytochemistry to evaluate the cells expressing NF-κB at 1.5 h following CO exposure. Compared to control, astrocytes prominently displayed greater GFAP and NF-κB p65 expression, and also NF-κB p65 nuclear co-localization (Fig. 4). The changes were diffuse, with no discernible differences among brain regions. We also found greater NF-κB p65 in microglia identified by expression of TMEM-119 (Fig. 5). There was no discernible NF-κB p65 expression in neurons identified by NPR expression.

3.4. Effects of inhibitors on CO-induced brain protein and MPs alterations

All brain protein changes identified in CO-exposed mice in Fig. 3 were abrogated if mice were injected prior to CO exposure with the MPO inhibitor, KYC (lane 3) or the NF-κB inhibitor, JSH-23 (lane 4). These interventions had no significant effect on protein content of air-breathing control mice in three replicate studies (data not shown). MPs elevations in cervical lymph nodes and blood of CO-exposed mice were also inhibited by KYC and JSH-23 injections, as shown in Fig. 6.

3.5. Effects of purified cervical node MPs injections

MPs from cervical lymph nodes were isolated from mice as described in section 2.3 and 60,000 injected via tail vein into naïve mice that had not been exposed to CO. Injections of node MPs from CO-exposed mice resulted in similar protein changes in brain as were seen in CO-exposed mice (Fig. 3, lane 5). Injections of node MPs from air-breathing, control mice had no significant effect on brain proteins in 3 replicate trials (data not shown). If node MPs from CO-exposed mice were injected into mice who had received KYC (Fig. 3, lane 6) or JSH-23 (lane 7) changes did not occur. Similarly, if MPs were first incubated with anti-TSP-1 blocking antibodies these changes did not occur (lane 8).

MPs injections also caused elevations in cervical lymph node and blood MPs similar to those seen among CO-exposed mice (Fig. 7). Notably, no changes in MPs number were identified when node MPs from control mice were injected into naïve mice, and MPs elevations were abrogated by if mice had received KYC or JSH-23, or when node MPs were incubated with anti-TSP-1 antibodies prior to injection.

3.6. Responses of CD36 knock-out mice

Fig. 8 demonstrates that CD36-KO mice showed no protein changes in brain when exposed to CO or when injected with node MPs isolated from wild type mice that had been exposed to CO. These mice also did not exhibit elevations of MPs in cervical nodes and blood in response to CO exposure (Fig. 6) or when injected with node MPs isolated from wild type mice that had been exposed to CO (Fig. 7).

3.7. CO causes neutrophil activation

Neutrophils obtained from the blood of mice subjected to CO exhibited increases in surface staining for CD18 (a component of β_2 integrins) as well as myeloperoxidase (MPO), consistent with cell activation/degranulation (Fig. 9). These changes were inhibited when mice had been injected with KYC or JSH-23 (Fig. 10 A). Virtually the same degree of activation was seen when naïve mice were injected with MPs isolated from cervical nodes of a CO-exposed mouse (Fig. 10 B). Neutrophil activation did not occur when node MPs were injected in mice who had received KYC, JSH-23 or if MPs were first incubated with anti-TSP-1 antibodies. We also did not identify activation of neutrophils from CO-exposed CD36-KO mice, or when CD36-KO mice were injected with node MPs isolated from wild type mice that had been exposed to CO.

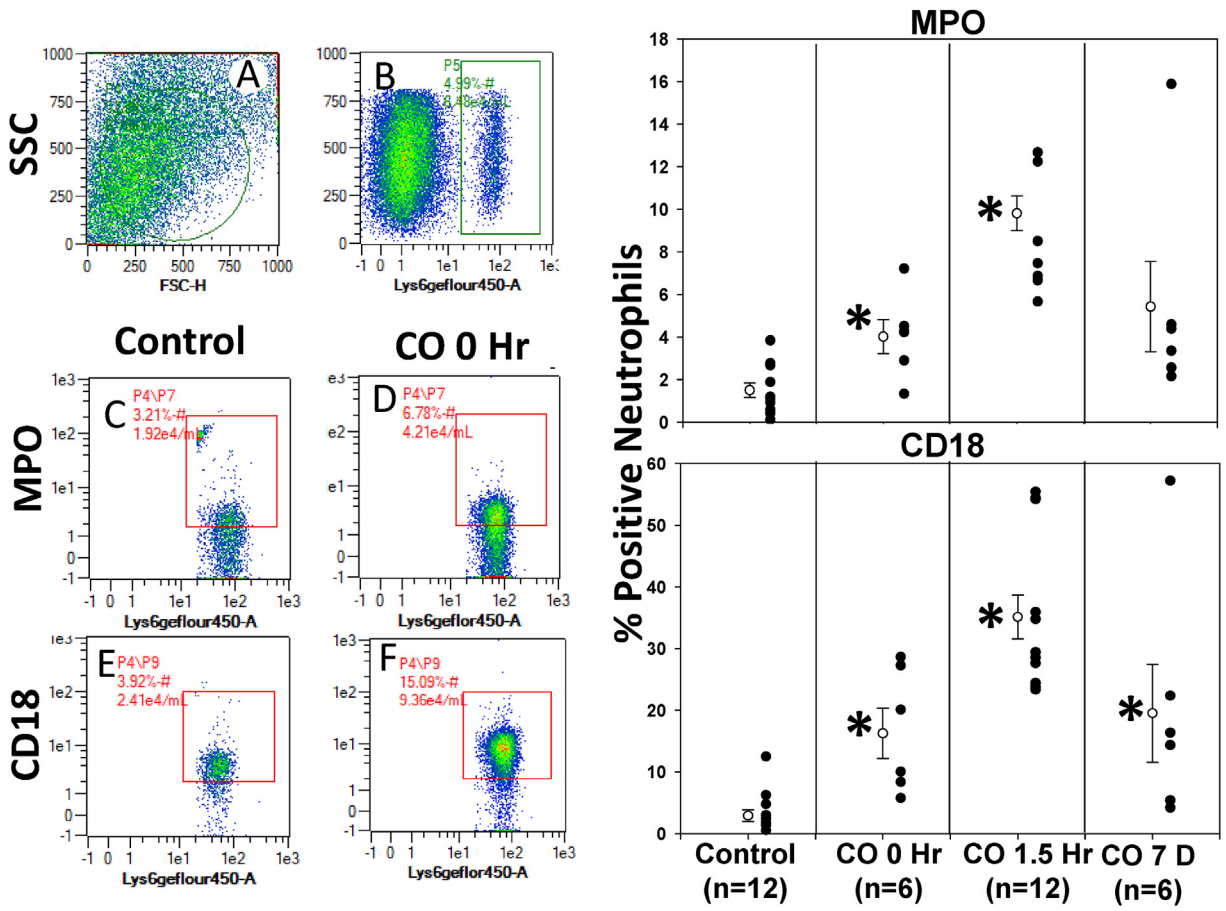

Fig. 9. Neutrophil activation. Neutrophils in whole blood were labeled by incubation with fluorophore-conjugated antibody to Ly6G and cell activation assessed by flow cytometry as co-expression of CD18 and MPO on the cell surface. Scatter diagrams to the left show the typical analysis approach where all cells are first plotted based on forward (FSC) and side (SSC) laser scatter (panel A), and the population that is labeled with Ly6G (neutrophils) is identified (panel B). MPO expression in the neutrophil populations from a control mouse (panel C) and a mouse exposed to CO (panel D) are quantified by the fraction of cells within the boxes. The box areas are established by control sequences run daily to determine positive staining (the fluorescence-minus-one process). The populations expressing CD18 are similarly shown in panels E and F.

The two panels on the right show the percent of neutrophils expressing MPO and CD18. The open circles show mean ± SE (replicate numbers are listed at the bottom of the figure) with * indicating those statistically significantly different from control ($p < 0.05$, ANOVA). Solid circles show individual data points for control and samples obtained from mice exposed to CO and then euthanized immediately, 1.5 h or 7 days after exposure.

3.8. Vascular leak occurs in brain and skeletal muscle post-CO

Vascular permeability to rhodamine-labeled dextran was significantly elevated in brain and skeletal muscle of mice euthanized at 1.5 h post-CO (Fig. 11). Vascular leakage in brain and muscle was inhibited when mice had been infused with KYC or JSH-23 prior to CO exposure, consistent with the absence of MPs elevations. However, Western blots using muscle homogenates failed to detect Ly6G or MPO in four replicate studies (these data not shown). This differs from Western blots of brain homogenates (Fig. 3), indicating an absence of neutrophil sequestration in muscle.

Vascular permeability changes were also found when naïve mice were injected with MPs isolated from cervical nodes of a CO-exposed mouse. These effects were inhibited when node MPs were injected into mice receiving KYC, JSH-23 or if MPs were first incubated with anti-TSP-1 antibodies, and no leakage was seen in CD36-KO mice exposed to CO or when injected with node MPs from a wild type CO-exposed mouse.

4. Discussion

All results from this investigation can be explained by a CO-induced cyclic neuroinflammatory process depicted in Fig. 1. We believe that CO first stimulates astrocytes because neutrophils are not directly activated by CO exposure (Thom, 1993). Astrocyte activation is supported by finding an elevation of GFAP-expressing MPs in the deep cervical lymph nodes (Fig. 2A). Increases in astrocyte GFAP, NF-κB and nuclear localization of NF-κB as shown in Fig. 4 are all consistent with cell activation (Sofroniew and Vinters, 2010).

Fig. 3 demonstrates that CO causes elevations of the p65 subunit of NF-κB and phospho-Ser^{536} p65 in brain. Inducible phosphorylation of NF-κB is considered a key mechanism in the positive regulation of NF-κB activity (Schmitz et al., 2004). Phosphorylation at serine 536 of the p65 subunit represents the site with the most potent inducible phosphorylation in response to inflammatory stimuli, and it is highly conserved among different species (Ghosh and Karin, 2002; Sakurai et al., 1999). The key role of NF-κB in the CO cycle is supported by the inhibitory effects of JSH-23. JSH-23 is an inhibitor of NF-κB nuclear translocation without affecting IκBα degradation (Kumar et al., 2011; Shin et al., 2004). As shown in Figs. 3, 6, 7, 10 and 11, JSH-23 inhibits all events triggered by CO exposure.

Exposure to CO increases the number of TSP-1 expressing MPs in deep cervical lymph nodes and also in blood (Fig. 2 A and B). As over 85% of TSP-1 MPs also express GFAP, the data suggest that TSP-1 MPs are generated by astrocytes. It appears that these MPs are responsible for activating neutrophils, as documented by flow cytometry (Fig. 10), because antibody to TSP-1 abrogates neutrophil activation associated with node MP injections. One consequence of neutrophil activation is

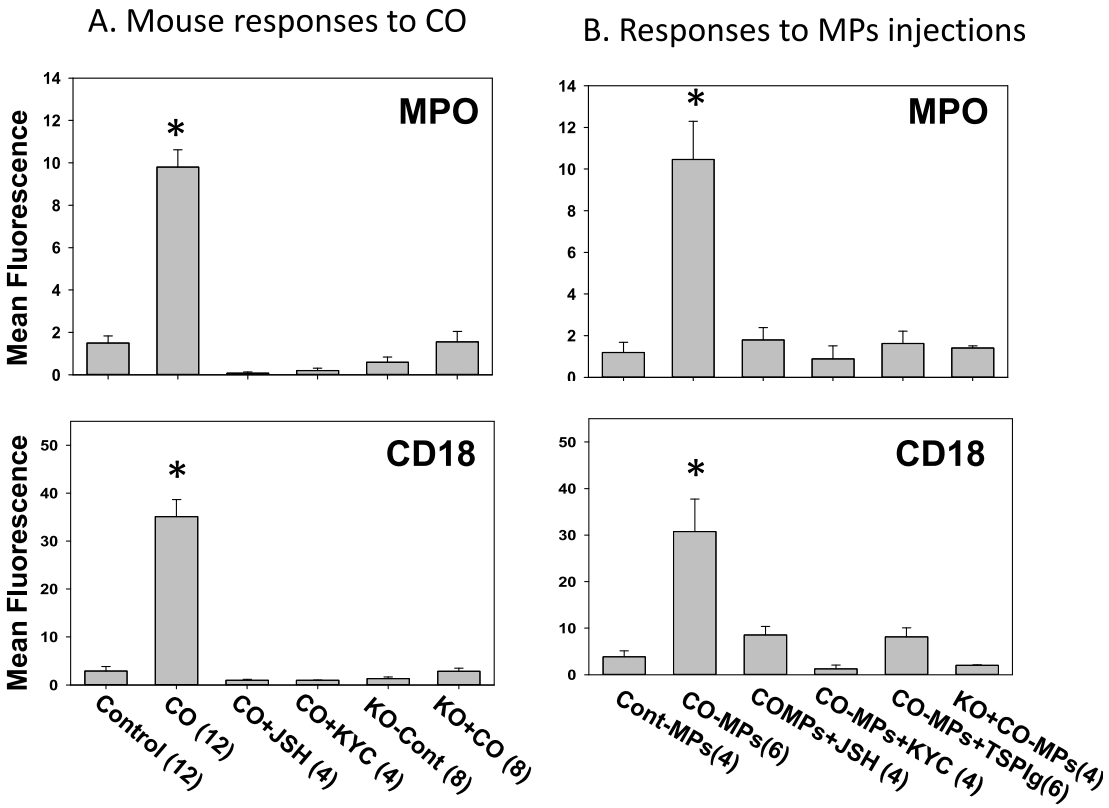

Fig. 10. Effects of interventions on neutrophil activation. Activation of neutrophils in whole blood from mice processed as described in Fig. 9 are shown as mean ± SE with replicate numbers shown at the bottom of the figure. Box plots are used to ease the ability to assess the differences among groups. Column A data reflect results from wild type control (air breathing) mice, and those euthanized 1.5 h following exposure to CO without and with JSH-23 or KYC. The last two columns in each figure show data from CD36 knock-out (KO) mice exposed only to air (Cont = control) or to CO. Column B show results from mice injected with 60,000 cervical lymph node MPs and euthanized 1.5 h later. Results are shown for wild type naïve mice injected with node MPs from wild type control mice (Cont-MPs), those injected with node MPs isolated from wild type control mice 1.5 h after exposure to CO (CO-MPs), those injected with CO-MPs and JSH-23, those injected with CO-MPs and KYC, and those injected with CO-MPs that were first incubated with IgG to TSP-1. The last column shows data from CD36 knock-out (KO) mice injected with CO-MPs. The * symbol indicates $p < 0.05$ versus the control, ANOVA.

MPs production, which was documented as an elevation in blood-borne MPs expressing Ly6G. It should be acknowledged, however, that not all Ly6G-expressing MPs need to have been generated by neutrophils. As is commonly seen (Thom et al., 2011; Yang et al., 2012), data in Fig. 2 A and B and Table 1 show that the % of MPs expressing proteins that are specific each cell type add up to well over 100%. Hence, MPs must interact and share surface proteins.

Neutrophils and MPO are indicated as leading back to astrocyte activation in Fig. 1 because we found elevations of Ly6G and MPO in brain homogenates of CO-exposed mice (Fig. 3). In prior studies we reported that immediately after animals are removed from a 1-h exposure to 1000 ppm CO, or more, MPO is detected in the brain vasculature and by 90 min β_2 integrin-dependent neutrophil sequestration occurs followed by protease release with endothelial xanthine dehydrogenase conversion to oxidase, oxidant production and brain lipid peroxidation (Ischiropoulos et al., 1996; Thom, 1993; Thom et al., 2006; Xu et al., 2013). The role of MPO with insult progression is supported by the inhibitory actions of KYC, a MPO inhibitor (Figs. 3, 6, 7, 10 and 11). In addition to exacerbating oxidative and nitrosative stresses, MPO at the vascular wall can also facilitate further neutrophil recruitment due to its positive surface charge (Klinke et al., 2011). Because neutrophil-derived MPs carry MPO, we interpret the significant elevation of MPO in excess of Ly6G in brain at 7 days post-CO, discussed in section 3.3, as indicative of perivascular MPs sequestration (Slater et al., 2017).

At 7- and 28-days post-CO we also found that MBP-bearing MPs were increased in cervical lymph nodes and blood (Fig. 2 A and B). This suggests ongoing oligodendrocyte stimulation. Further work will be needed to assess whether these particles contribute to neuroinflammation, given evidence for an adaptive immunological response to MBP post-CO (Thom et al., 2004, 2006). It appears that oxidant-modified MBP primes lymphocytes that along with macrophage/microglial activation and lymphocyte influx leads to neurological impairments (Han et al., 2007; Thom et al., 2004, 2006).

CD36 elevations in brain following CO exposure are shown in Fig. 3. NF-κB activation can enhance CD36 expression and endothelial CD36 engagement enhances NF-κB activation and neutrophil recruitment (Cho et al., 2005; Kim et al., 2015; Kunz et al., 2008; Panicker et al., 2019). We show this in Fig. 1 as a double arrow between astrocytes and endothelium. CD36 KO mice were resistant to CO-induced biochemical events in brain, MPs production and neutrophil activation. These mice demonstrate the same resistance in response to injections of node MPs from CO-exposed wild type mice (Figs. 6–8, 10,11). CD36 is a receptor for TSP-1, and antibodies to TSP-1 inhibited responses triggered by cervical node MPs injections in wild-type mice. Therefore, the data indicate that CD36 plays a central role in progression of CO-induced neuroinflammation.

Finding that MPs injections elevated p65 NF-κB and phospho-Ser^{536} p65 in brain (Fig. 3) once again supports a cyclic process triggered by CO, and an astrocyte response to intravenous MPs injections is reflected by the large increase in cervical node GFAP/TSP-1 expressing MPs (Figs. 2B and 7). Inhibition of these responses by JSH-23 suggests an endothelium-to-astrocyte communication, given that there would not be a direct interaction of MPs with astrocytes to induce NF-κB activation. Future work with conditional deletion of CD36 on either endothelium or astrocytes will be required to discern the roles of endothelium versus astrocytes in CO poisoning.

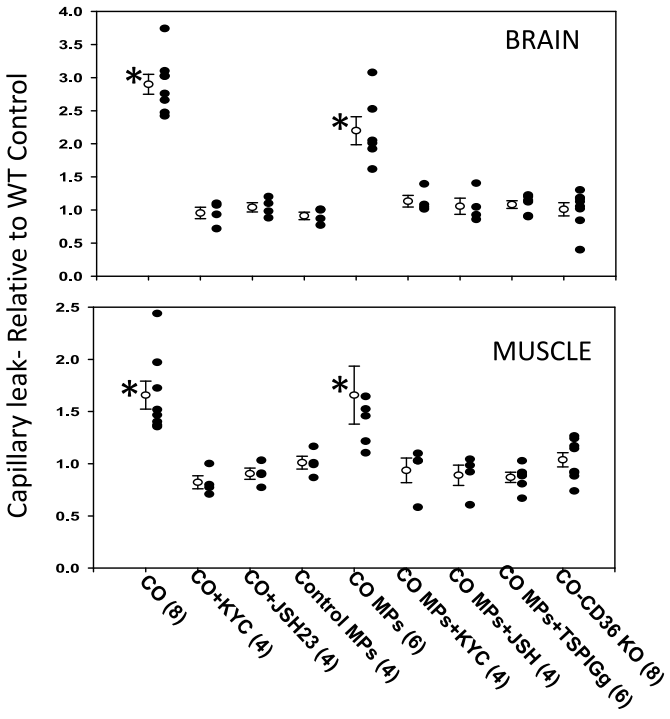

Fig. 11. Vascular leakage of 2×10^6 Da rhodamine-labeled dextran was assessed for brain and leg skeletal muscle prepared and evaluated as described in section 2.8. Values reflect the fluorescence from rhodamine normalized to values for tissues from control mice. Data show mean ± SE (open circles) with individual data points (solid circles) for mice euthanized 1.5 h following exposure to CO without and with JSH-23 or KYC, wild type naïve mice injected with 60,000 cervical node MPs from air-breathing control mice (Control-MPs), wild type naïve mice injected with node MPs from wild type mice 1.5 h after exposure to CO (CO-MPs), those injected with CO-MPs as well as KYC or JSH-23, and those injected with CO-MPs that were first incubated with IgG to TSP-1. The last column shows data from CD36 knock-out (KO) mice injected with CO-MPs. Data are mean ± SE, n is shown for each sample, * indicates significantly different from control, $p < 0.05$, ANOVA.

Reciprocal communications between endothelium and astrocytes can establish a chronic neuroinflammatory state, as is seen in other disorders (Hsiao et al., 2013). The presence of CD36 on endothelium and communication with astrocytes may explain why in response to CO exposure, neutrophils target the neurovasculature. Vascular damage due to CO was directly demonstrated as leakage of 2×10^6 Da rhodamine-dextran (Fig. 11). In prior work we linked CO-induced neurovascular damage to prolongation of neuronal action potential (Xu et al., 2013). We think it notable that a modest vascular leak was identified in skeletal muscle, but Western blots did not indicate neutrophil sequestration as increases of Ly6G and MPO. Vascular leak in muscle did not occur in CD36 KO mice or in KO mice injected with cervical node MPs from CO-exposed wild type mice, thus indicating a role for the CD36 receptor. We conclude that TSP-1 expressing MPs cause skeletal muscle dextran leakage because it was inhibited when MPs were injected in combination with anti-TSP antibodies. TSP-1 enhances endothelial permeability by influencing vascular endothelial growth factor receptor function and permeability is not increased by TSP-1 in CD36 KO mice (Zhang et al., 2009). Therefore, our findings indicate that endothelial cell activation with production of a vascular leak is not a sufficient stimulus to trigger neutrophil sequestration. Hence, neutrophil sequestration at the neurovasculature but not at muscle in the peripheral circulation post-CO appears to be due to the close association between brain endothelium and astrocytes, with inflammatory responses linked to NF-κB.

Others have reported CD36 elevations intrinsic to endothelial cells and microglia at 24–72 h following ischemia-reperfusion, whereas we see changes within 1.5 h (Cho et al., 2005). We suspect the elevation following CO is related in part to local production by endothelium, astrocytes and microglia, but the rapid increase is likely due to recruited monocytes as they normally carry CD36. CD36 elevations in brain due to leukocyte influx is a process that has been described by others (Kim et al., 2012), and we have reported macrophage/microglial and lymphocyte activation and leukocyte influx into brain occurs with CO poisoning (Thom et al., 2004). Neutrophil sequestration cannot explain the rapid elevation of CD36 in brain because these cells normally express little CD36 and increased cell production is variable among alternative stimuli (Ericson et al., 2014; Greenwalt et al., 1992).

Progressive neuroinflammation leads to loss of AQP4 or at least diminished antibody recognition with CO poisoning (Fig. 3), a phenomenon also reported by others (Wei et al., 2019). As this was inhibited by KYC, we interpret the change in AQP4 as a response to perivascular oxidative and nitrosative stress triggered by neutrophil sequestration and MPO activity. Perturbation of AQP4 is expected to disturb glymphatic function and we are investigating whether this occurs post-CO. AQP4 impairment leads to glymphatic dysfunction in aging, traumatic brain injury, Alzheimer's disease, ischemic and hemorrhagic stroke (Rasmussen et al., 2018). Occult glymphatic dysfunction is speculated to be the basis for a variety of demyelinating diseases (Barz et al., 2017). MRI changes common to CO poisoning are often seen in those with glymphatic dysfunction (Jeon et al., 2018; Varrassi et al., 2017). It remains to be determined whether such changes relate to the elevation of MBP-containing MPs seen 1–4 weeks following CO exposure (Fig. 2 A and B).

Others have commented that processes extrinsic to brain structures could contribute to delayed leukoencephalopathy with CO and other agents (Beppu, 2014; Sprecher and Mehta, 2010). The role for neutrophils in CO-induced neuroinflammation is consistent with these observations. The cycle described in Fig. 1 may explain why COHb is a poor index of neurological risk. As MPs elevations in response to CO persist for at least 4 weeks (Fig. 2 A and B), neuroinflammation appears to be an ongoing process. These data offer a possible explanation for why neurological dysfunction sometimes appears in a delayed fashion, as long-term neuroinflammation is viewed as a central factor in neurotoxicity of many disorders (Block et al., 2007). So-called delayed neurological deterioration can be ascribed to CO poisoning for up to 5–6 weeks post-exposure (Sprecher and Mehta, 2010).

One aspect of our findings that is not well explained is the absence of neutrophil activation when CD36 KO mice are injected with cervical node MPs from CO-exposed wild type mice (Fig. 10B). CD36 expression is negligible on unstimulated neutrophils (Ericson et al., 2014; Greenwalt et al., 1992), but there are multiple other TSP-1 receptors on these cells, so we had expected the MPs to activate KO mouse neutrophils. Absence of this response could arise if, rather than occurring due to TSP-1 expressing MPs, neutrophil activation following MPs injections is actually due to alternative pro-inflammatory agents generated after endothelial CD36 engagement when the cyclic neuroinflammatory process is initiated. Endothelial CD36 engagement leads to expression of granulocyte colony-stimulating factor that is responsible for neutrophil neurotoxicity in relation to ischemic brain injury (Garcia-Bonilla et al., 2015). As shown in Figs. 6 and 7, brain inflammatory responses such as the myriad MPs expressing brain-specific proteins are not generated in CD36 KO mice exposed to CO or when KO mice are injected with cervical node MPs from wild type CO-exposed mice. Further work is needed to resolve this question.

Finally, the cyclic process illustrated in Fig. 1 may be a common feature with brain injuries and not unique to CO. MPs and other extracellular vesicles generated systemically can exacerbate traumatic and other causes of brain injury and reciprocally, CNS-derived MPs cause peripheral vascular disorders once liberated to the blood stream (Kumar et al., 2017; Yang et al., 2013; Zhao et al., 2017). Further studies are required to provide experimental evidence for this hypothesis.

The translational relevance of our study is obviously limited because a

murine model was used. However, this model does demonstrate the role of MBP in CO-induced neuroinflammation (Thom et al., 2004). MBP has since been implicated in development of delayed neurological sequelae in humans based on its appearance in the cerebrospinal fluid of symptomatic patients (Beppu et al., 2012; Ide and Kamijo, 2009; Kamijo et al., 2007; Kuroda et al., 2016). Plans are underway to investigate blood-borne MPs in CO-poisoned patients using some of the same methods we have used in other clinical studies (Thom et al., 2015). Importantly, results from the current study suggest a number of possible therapeutic opportunities because of the on-going nature of CO-induced neuroinflammation lasting weeks and the cyclic mechanism between blood-borne and CNS leukocytes. Currently, there is no effective treatment for CO-induced neurological sequelae.

Declaration of competing interest

The author(s) declare no competing interests.

Acknowledgements

This project was supported by Grant N00014-16-1-2868 from the Office of Naval Research and an unrestricted grant from the National Foundation of Emergency Medicine.

References

Absinta, M., Ha, S.K., Nair, G., 2017. Human and nonhuman primate meninges harbor lymphatic vessels that can be visualized noninvasively by MRI. Elife 6, e29738.
Bai, B., Yang, Y., Wang, Q., Li, M., Tian, C., Liu, Y., UAung, L.H.H., Li, P.F., Yu, T., Chu, X.M., 2020. NLRP3 inflammasome in endothelial dysfunction. Cell Death Dis. 11, 776.
Barz, H., Schreiber, A.D., Barz, U., 2017. Demyelinating diseases as a result of cerebral edema? Med. Hypotheses 104, 10–14.
Beaulieu, E., Demeule, M., Ghitescu, L., Beliveau, R., 1997. P-glycoprotein is strongly expressed in the luminal membranes of the endothelium of blood vessels in the brain. Biochem. J. 326, 539–544.
Beppu, T., 2014. The role of MR imaging in assessment of brain damage from carbon monoxide poisoning: a review of the literature. AJNR Am J Neuroradiol 35, 625–631.
Beppu, T., Fujiwara, S., Nishimoto, H., Koeda, A., Narumi, A., Mori, K., Ogasawara, K., Sasaki, M., 2012. Fractional anisotropy in the centrum semiovale as a quantitative indicator of cerebral white matter damage in the subacute phase in patients with carbon monoxide poisoning: correlation with the concentration of myelin basic protein in cerebrospinal fluid. J. Neurol. 259, 1698–1705.
Bhullar, J., Bhopale, V.M., Yang, M., Sethuraman, K., Thom, S.R., 2016. Microparticle formation by platelets exposed to high gas pressures – an oxidative stress response. Free Radic. Biol. Med. 101, 154–162.
Block, M.L., Zecca, L., Hong, J.S., 2007. Microglia-mediated neurotoxicity: uncovering the molecular mechanisms. Nat. Rev. Neurosci. 8, 57–69.
CDC, C.f.D.C., 2007. Carbon monoxide-related deaths-United States, 1999-2004. MMWR Morb. Mortal. Wkly. Rep. 56, 1309–1312.
Cho, S., Park, E.M., Febbraio, M., Anrather, J., Park, L., Racchumi, G., Silverstein, R.L., Iadecola, C., 2005. The class B scavenger receptor CD36 mediates free radical production and tissue injury in cerebral ischemia. J. Neurochem. 25, 2504–2512.
Ericson, J.A., Duffau, P., Yasuda, K., Ortiz-Lopez, A., Rothamel, K., Rifkin, I.R., Monach, P.A., Consortium, I., 2014. Gene expression during the generation and activation of mouse neutrophils: implication of novel functional and regulatory pathways. PLoS One 9, e108553.
Febbraio, M., Silverstein, R.L., 2007. CD36: implications in cardiovascular disease. Int. J. Biochem. Cell Biol. 39, 2012–2030.
Garcia-Bonilla, L., Racchumi, G., Murphy, M., Anrather, J., Iadecola, C., 2015. Endothelial CD36 contributes to postischemic brain injury by promoting neutrophil activation via CSF3. J. Neurosci. 35, 14783–14793.
Ghosh, A., Li, W., Febbraio, M., Espinola, R.G., McCrae, K., Silverstein, R.L., 2008. Platelet CD36 mediates interactions with endothelial cell-derived microparticles and contributes to thrombosis in vivo. J. Clin. Invest. 118, 1934–1943.
Ghosh, S., Karin, M., 2002. Missing pieces in the NF-kappaB puzzle. Cell 109 (Suppl. l), S81–S96.
Greenwalt, D.E., Lipsky, R.H., Ockenhouse, C.F., H I, Tandon, N.N., Jamieson, G.A., 1992. Membrane glycoprotein CD36: a review of its roles in adherence, signal transduction, and transfusion medicine. Blood 80, 1105–1115.
Hampson, N.B., 2016a. U.S. mortality due to carbon monoxide poisoning, 1999-2014: accidental and intentional deaths. Ann. Am Thorac. Soc. 13, 1768–1774.
Hampson, N.B., Piantadosi, C.A., Thom, S.R., Weaver, L.K., 2012. Practice recommendations in the diagnosis, management, and prevention of carbon monoxide poisoning. Am. J. Respir. Crit. Care Med. 186, 1095–1101.
Hampson, N.B., 2016b. Cost of accidental carbon monoxide poisoning: a preventable expense. Prev. Med. Rep. 3, 667–685.
Han, S.T., Bhopale, V.M., Thom, S.R., 2007. Xanthine oxidoreductase and neurological sequelae of carbon monoxide poisoning. Toxicol. Lett. 170, 111–115.
Holter, K.E., Kehlet, B., Devor, A., Sejnowski, T.J., Dale, A.M., Omholt, S.W., POttersen, O.P., Nagelhus, E.A., Mardal, K.A., Pettersen, K.H., 2017. Interstitial solute transport in 3D reconstructed neuropil occurs by diffusion rather than bulk flow. Proc. Natl. Acad. Sci. Unit. States Am. 114, 9894–9899.
Hsiao, H.Y., Chen, Y.C., Chen, H.M., Tu, P.H., Chern, Y., 2013. A critical role of astrocyte-mediated nuclear factor-kB-dependent inflammation in Huntington's disease. Hum. Mol. Genet. 22, 1826–1842.
Ide, T., Kamijo, Y., 2009. The early elevation of interleukin 6 concentration in cerebrospinal fluid and delayed encephalopathy of carbon monoxide poisoning. Am. J. Emerg. Med. 27, 992–996.
Iliff, J.J., Wang, M., Liao, Y., Plogg, B.A., Peng, W., 2012. A paravascular pathway facilitates CSF flow through the brain parenchyma and the clearance of interstitial solutes, including amyloid β. Sci. Transl. Med. 4, 147ra111.
Ischiropoulos, H., Beers, M.F., Ohnishi, S.T., Fisher, D., Garner, S.E., Thom, S.R., 1996. Nitric oxide production and perivascular tyrosine nitration in brain after carbon monoxide poisoning in the rat. J. Clin. Invest. 97, 2260–2267.
Jeon, S.B., Sohn, C.H., Seo, D.W., Oh, B.J., Lim, K.S., Kang, D.W., Kim, W.Y., 2018. Acute brain lesions on magnetic resonance imaging and delayed neurological sequelae in carbon monoxide poisoning. JAMA Neurol 75, 436–443.
Kamijo, Y., Soma, K., Ide, T., 2007. Recurrent myelin basic protein elevation in cerebrospinal fluid as a predictive marker of delayed encephalopathy after carbon monoxide poisoning. Am. J. Emerg. Med. 25, 483–485.
Kang, S., Byun, J., Non, S.M., Mook-Jung, I., 2018. Thrombospondin-1 protects against Aβ-induced mitochondrial fragmentation and dysfunction in hippocampal cells. Cell Death Discovery 4, 31.
Kim, E., Febbraio, M., Bao, Y., Tolhurst, A.T., Epstein, J.M., Cho, S., 2012. CD36 in the periphery and brain synergizes in stroke injury in hyperlipidemia. Ann. Neurol. 71, 753–764.
Kim, E.H., Tolhurst, A.T., Szetea, H.H., Cho, S.H., 2015. Targeting CD36-mediated inflammation reduces acute brain injury in transient, but not permanent, ischemic stroke. CNS Neurosci. Ther. 21, 385–391.
Klinke, A., Nussbaum, C., Kubala, L., Friedrichs, K., Rudolph, T.K., Rudolph, V., Paust, H.J., Schroder, C., Benten, D., Lau, D., Szocs, K., Furtmuller, P.G., Heerings, P., Sydow, K., Duchstein, H.J., Ehmke, H., Schumacher, U., Meinertz, T., Sperandio, M., Baldus, S., 2011. Myeloperoxidase attracts neutrophils by physical forces. Blood 117, 1350–1358.
Kumar, A., Negi, G., Sharma, S.S., 2011. JSH-23 targets nuclear factor-kappa B and reverses various deficits in experimental diabetic neuropathy: effect on neuroinflammation and antioxidant defence. Diabetes Obes. Metabol. 13, 750–758.
Kumar, A., Stoica, B.A., Loane, D.J., Yang, M., Abulwerdi, G., Khan, N., Kumar, A., Thom, S.R., Faden, A.I., 2017. Microglial-derived microparticles mediate neuroinflammation after traumatic brain injury. J. Neuroinflammation 14 (47), 1–17. https://doi.org/10.1186/s12974-017-0819-4.
Kunz, A., Abe, T.A., Hochrainer, K., Shimamura, M., Anrather, J., Racchumi, G., Zhou, P., Iadecola, C., 2008. Nuclear factor-kB activation and postischemic inflammation are suppressed in CD36-null mice after middle cerebral artery occlusion. J. Neurosci. 28, 1649–1658.
Kuroda, H., Fujihara, K., Mugikura, S., Takahashi, S., Kushimoto, S., Aoki, M., 2016. Altered white matter metabolism in delayed neurologic sequelae after carbon monoxide poisoning: a proton magnetic resonance spectroscopic study. J. Neurol. Sci. 360, 161–169.
Lu, Z., Kipnis, J., 2010. Thrombospondin 1–a key astrocyte-derived neurogenic factor. Faseb. J. 24, 1925–1934.
Majluf-Cruz, A., Manns, J.M., Uknis, A.B., TYang, X., Comlman, R.W., Harris, R.B., Frazier, W., Lawler, J., DeLa Cadena, R.A., 2000. Residues F16-G33 and A784-N823 within platelet thrombospondin-1 play a major role in binding human neutrophils: evaluation by two novel binding assays. J. Lab. Clin. Med. 136, 292–302.
Martin-Manso, G., Galli, S., Ridnour, L.A., Tsokos, M., Wink, D.A., Roberts, D.D., 2000. Thrombospondin 1 promotes tumor macrophage recruitment and enhances tumor cell cytotoxicity of differentiated U937 cells. Cancer Res. 68, 7090–7099.
Mattiuzzi, C., Lippi, G., 2020. Worldwide epidemiology of carbon monoxide poisoning. Hum. Exp. Toxicol. 39, 387–392.
Mause, S.F., Weber, C., 2010. Microparticles: protagonists of a novel communication network for intercellular information exchange. Circ. Res. 107, 1047–1057.
Panicker, N., Sarkar, S., Harischandra, D.S., Neal, M.D., Kam, T.I., Jin, H.K., Saminathan, H., Langley, M., Charli, A., Samidurai, M., Rokad, D., Ghaisas, S., Pletnikova, O., Dawson, V.L., Dawson, T.M., Anantharam, V., Kanthasamy, A.G., Kanthasamy, A., 2019. Fyn kinase regulates misfolded α-synuclein uptake and NLRP3 inflammasome activation in microglia. J. Exp. Med. 216, 1411–1430.
Rasmussen, M.K., Humberto, M., Nedergaard, M., 2018. The glymphatic pathway in neurological disorders. Lancet Neurol. 17, 1016–1024.
Raub, J.A., Mathieu-Nolf, M., Hampson, N.B., Thom, S.R., 2000. Carbon monoxide poisoning–a public health perspective. Toxicology 145, 1–14.
Rose, J.J., Wang, L., Xu, Q., McTiernan, C.F., Shiva, S., Tejero, J., Gladwin, M.T., 2017. Carbon monoxide poisoning: pathogenesis, management, and future directions of therapy. Am. J. Respir. Crit. Care Med. 195, 596–606.
Ruhela, D., Bhopale, V.M., Yang, M., Yu, K., Weintraub, E., Greenblatt, A., Thom, S.R., 2020. Blood-borne and brain-derived microparticles in morphine-induced anti-nociceptive tolerance. Brain Behav. Immun. 87, 465–472.
Sakurai, H., Chiba, H., Miyoshi, H., Sugita, T., Toriumi, W., 1999. IkappaB kinases phosphorylate NF-kappaB p65 subunit on serine 536 in the transactivation domain. J. Biol. Chem. 274, 30353–30356.
Schmitz, M.L., Mattioli, I., Buss, H., Kracht, M., 2004. NF-kappaB: a multifaceted transcription factor regulated at several levels. Chembiochem 5, 1348–1358.

Shin, H.M., Kim, M.H., Kim, B.H., Jung, S.H., Kim, Y.S., Park, H.J., Hong, J.T., KMin, K.R., Kim, Y., 2004. Inhibitory action of novel aromatic diamine compound on lipopolysaccharide-induced nuclear translocation of NF-kB without affecting IkB degradation. FEBS Lett. 571, 50–54.

Silverstein, R.L., Febbraio, M., 2009. CD36, a scavenger receptor involved in immunity, metabolism, angiogenesis, and behavior. Sci. Signal. 2, re3.

Slater, T.W., Finkielsztein, A., Mascarenhas, L.A., Mehl, L.C., Butin-Israeli, V., Sumagin, R., 2017. Neutrophil microparticles deliver active myeloperoxidase to injured mucosa to inhibit epithelial wound healing. J. Immunol. 198, 2886–2897.

Sofroniew, M.V., Vinters, H.V., 2010. Astrocytes: biology and pathology. Acta Neuropathol. 119, 7–35.

Sprecher, D., Mehta, L., 2010. The syndrome of delayed post-hypoxic leukoencephalopathy. NeuroRehabilitation 26, 65–72.

Thom, S.R., 1990. Carbon monoxide-mediated brain lipid peroxidation in the rat (1985). J. Appl. Physiol. 68, 997–1003.

Thom, S.R., 1992. Dehydrogenase conversion to oxidase and lipid peroxidation in brain after carbon monoxide poisoning (1985). J. Appl. Physiol. 73, 1584–1589.

Thom, S.R., 1993. Leukocytes in carbon monoxide-mediated brain oxidative injury. Toxicol. Appl. Pharmacol. 123, 234–247.

Thom, S.R., Bennett, M., Banham, N.D., Chin, W., Blake, D.F., Rosen, A., Pollock, N.W., Madden, D., Barak, O., Marroni, A., Balestra, C., Germonpre, P., Pieri, M., Cialoni, D., Le, P.N., Logue, C., Lambert, D., Hardy, K.R., Sward, D., Yang, M., Bhopale, V.B., Dujic, Z., 2015. Association of microparticles and neutrophil activation with decompression sickness (1985). J. Appl. Physiol. 119, 427–434.

Thom, S.R., Bhopale, V.M., Fisher, D., Zhang, J., Gimotty, P., 2004. Delayed neuropathology after carbon monoxide poisoning is immune-mediated. Proc. Natl. Acad. Sci. U. S. A. 101, 13660–13665.

Thom, S.R., Bhopale, V.M., Han, S.T., Clark, J.M., Hardy, K.R., 2006. Intravascular neutrophil activation due to carbon monoxide poisoning. Am. J. Respir. Crit. Care Med. 174, 1239–1248.

Thom, S.R., Bhopale, V.M., Hu, J., Yang, M., 2017a. Increased carbon dioxide levels stimulate neutrophils to produce microparticles and activate the nucleotide-binding domain-like receptor 3 inflammasome. Free Radic. Biol. Med. 106, 406–416.

Thom, S.R., Bhopale, V.M., Yang, M., 2014. Neutrophils generate microparticles during exposure to inert gases due to cytoskeletal oxidative stress. J. Biol. Chem. 289, 18831–18845.

Thom, S.R., Bhopale, V.M., Yu, K., Huang, W., Kane, M.A., Margolis, D.J., 2017b. Neutrophil microparticle production and inflammasome activation by hyperglycemia due to cytoskeletal instability. J. Biol. Chem. 292, 18312–18324.

Thom, S.R., Fisher, D., Xu, Y.A., Garner, S., Ischiropoulos, H., 1999. Role of nitric oxide-derived oxidants in vascular injury from carbon monoxide in the rat. Am. J. Physiol. 276, H984–H992.

Thom, S.R., Taber, R.L., Mendiguren II, Clark, J.M., Hardy, K.R., Fisher, A.B., 1995. Delayed neuropsychologic sequelae after carbon monoxide poisoning: prevention by treatment with hyperbaric oxygen. Ann. Emerg. Med. 25, 474–480.

Thom, S.R., Yang, M., Bhopale, V.M., Huang, S., Milovanova, T.N., 2011. Microparticles initiate decompression-induced neutrophil activation and subsequent vascular injuries (1985). J. Appl. Physiol. 110, 340–351.

Tian, W., Sawyer, A., F B, K., Kyriakides, T.R., 2011. Astrocyte-derived thrombospondin-2 is critical for the repair of the blood-brain barrier. Am. J. Pathol. 179, 860–868.

Varrassi, M., Di Sibio, A., Gianneramo, C., Perri, M., Saltelli, G., Splendiani, A., Masciocchi, C., 2017. Advanced neuroimaging of carbon monoxide poisoning. NeuroRadiol. J. 30, 461–469.

Verkhratsky, A., Matteoli, M., Parpura, V., Mothet, J.P., Zorec, R., 2016. Astrocytes as secretory cells of the central nervous system: idiosyncrasies of vesicular secretion. EMBO J. 35, 239–257.

Wei, F., Song, J., Zhang, C.,]Lin, J., Xue, R., Shan, L.D., Gong, S., Zhang, G.X., Qin, Z.H., Xu, G.Y., Wang, L.H., 2019. Chronic stress impairs the aquaporin-4-mediated glymphatic transport through glucocorticoid signaling. Psychopharmacology 236 (4), 1367–1384. https://doi.org/10.1007/s00213-018-5147-6.

Weller, R.O., Subash, M., Preston, S.D., Mazanti, I., Carare, R.O., 2008. Perivascular drainage of amyloid-b peptides from the brain and its failure in cerebral amyloid angiopathy and Alzheimer's Disease. Brain Pathol. 18, 253–266.

Won, W.J., Bachmann, M.F., Kearney, J.F., 2008. CD36 is differentially expressed on B cell subsets during development and in responses to antigen. J. Immunol. 180, 230–237.

Xu, J., Yang, M., Kosterin, P., Salzberg, B.M., Milovanova, T.N., Bhopale, V.M., Thom, S.R., 2013. Carbon monoxide inhalation increases microparticles causing vascular and CNS dysfunction. Toxicol. Appl. Pharmacol. 273, 410–417.

Yang, M., Kosterin, P., Salzberg, B.M., Milovanova, T.N., Bhopale, V.M., Thom, S.R., 2013. Microparticles generated by decompression stress cause central nervous system injury manifested as neurohypophiseal terminal action potential broadening. J. Appl. Physiol. 115, 1481–1486.

Yang, M., Milovanova, T.N., Bogush, M., Uzun, G., Bhopale, V.M., Thom, S.R., 2012. Microparticle enlargement and altered surface proteins after air decompression are associated with inflammatory vascular injuries (1985). J. Appl. Physiol. 112, 204–211.

Zhang, H., Ray, A., Miller, N.M., Hartwig, D., Pritchard, K.A., Dittel, B.N., 2016. Inhibition of myeloperoxidase at the peak of exerimental autoimmune encephalomyelitis restores blood-brain barrier integrity and ameliorates disease severity. J. Neurochem. 136, 826–836.

Zhang, X., Kazerounian, S., Duquette, M., Perruzzi, C., Nagy, J.A., Dvorak, H.F., Parangi, S., Lawler, J., 2009. Thrombospondin-1 modulates vascular endothelial growth factor activity at the receptor level. Faseb. J. 23, 3368–3376.

Zhao, Z., Zhou, Y., Tian, Y., Li, M., Dong, J.F., Zhang, J., 2017. Cellular microparticles and pathophysiology of traumatic brain injury. Protein Cell 8, 801–810.